A High-Payload Proprioceptive Hybrid Robotic Gripper With Soft Origamic Actuators

Yinyin Su, Zhonggui Fang ⬡, Wenpei Zhu, Xiaochen Sun ⬡, Yuming Zhu ⬡, Hexiang Wang, Kailuan Tang,
Hailin Huang ⬡, Sicong Liu ⬡, and Zheng Wang ⬡, *Senior Member, IEEE*

Abstract—**Proprioception is the ability to perceive environmental stimulations through internal sensory organs. Enabling proprioception is critical for robots to be aware of the environmental interactions and respond appropriately, particularly for high-payload grippers to ensure safety when handling delicate objects. State-of-the-art robotic grippers with soft actuators are typically equipped with pressure sensors for pneumatic regulation and control, but very few utilized them for proprioceptive purposes. This lack of environmental awareness was largely compensated by their inherent compliance and conformity, but also due to the generally limited force capabilities. Targeting at this gap, this work proposes a novel Proprioceptive Origamic Soft Actuator (POSA) joint, and a corresponding hybrid robotic gripper design with high-payload soft origamic actuators and rigid supporting frames, achieving up to 564.5 N actuator output force or 302.4 N finger gripping force at 150 kPa low pneumatic pressure and 3.2 kg self-weight. Despite the substantially higher force capability over state-of-the-art soft grippers, the proposed hybrid gripper could retain the excellent inherent compliance thanks to the novel soft origamic actuators. Moreover, a novel scheme of multi-actuator proprioception is proposed by only using the embedded pneumatic pressure sensors, to enable the hybrid gripper with environmental awareness, achieving real-time position and force estimations of errors at $<1\%$ and 5.6%, respectively. The principles, design, prototyping, and experiments of the proposed hybrid high-payload gripper were presented in this letter. Combining soft robotic compliance, high payload, and proprioception, the gripper could both hold a pealed grape and crack a walnut, with position and force signals being measured without requiring dedicated sensors.**

Index Terms—**Hybrid robotic gripper, soft origamic actuators, POSA joint, higher force capability, proprioception.**

Yinyin Su, Zhonggui Fang, Wenpei Zhu, Xiaochen Sun, Yuming Zhu, Kailuan Tang, and Sicong Liu are with the Department of Mechanical and Energy Engineering, Southern University of Science and Technology, Shenzhen 518000, China (e-mail: yinyinsu1991@gmail.com; 11930523@mail.sustech.edu.cn; 11930368@mail.sustech.edu.cn; xiaochensun1995@163.com; 11711107@mail.sustech.edu.cn; 11949019@mail.sustech.edu.cn; liusc@sustech.edu.cn).

Hexiang Wang and Hailin Huang are with the Department of Mechanical Engineering, Harbin Institute of Technology (Shenzhen), Shenzhen 518055, China (e-mail: 180310303@stu.hit.edu.cn; huanghitsz@gmail.com).

Zheng Wang is with the Department of Mechanical and Energy Engineering, Southern University of Science and Technology, Shenzhen 518000, China, and also with the Department of Mechanical Engineering, The University of Hong Kong, Hong Kong (e-mail: zheng.wang@ieee.org).

Digital Object Identifier 10.1109/LRA.2020.2974438

I. INTRODUCTION

ROBOTIC grippers have been widely adopted in various application scenarios by directly contacting objects, or interacting with humans for home assistance and elderly care [1], [2]. Rigid mechanical structures commonly used for conventional robotic grippers achieved excellent precision and large forces [3]. Incorporating sensory control, compliance and force control could be achieved [2]. However, the real-world unstructured environments bring specific challenges to rigid grippers, such as grasping irregular or fragile items dynamically [1], [4]–[6], where soft robotic grippers emerging recently excel with their intrinsic compliance [7], [8]. With their unique properties of lower stiffness and continuous deformation, soft grippers grasp various objects with simple structure and control, reducing the complexity and system cost significantly, while improving safety [4], [9]–[11]. Unlike their electric-motor-driven counter parts, soft grippers are usually actuated by pneumatics, hydraulics, cable-drive actuation, shape memory alloys, electroactive polymers, as well as electrohydraulics. [3], [12]–[14]. Specifically, pneumatic artificial muscles (PAMs) have been widely adopted in soft grippers [15], [16]. Origami-based soft actuators have also been reported for gripper design [17], [18].

However, soft grippers also inherit the general limitations of soft robots, from limited repeatability, precision, to low grasping force and speed, significantly restricting their wider application [3], [13], [19]. Several approaches have been proposed to improve load capacity, from gecko-inspired adhesives [20], shape memory alloy (SMA) [21], achieving higher payload while compromising control simplicity and response time [19]. Sensory feedback is also essential for motion and force control [2]. Pioneering works have been reported, including embedding magnetic curvature sensors in bidirectional bending actuators [22], and using conductive liquids as proprioceptive sensor [23], requiring dedicated sensory elements to measure each feedback modality.

This work proposed a novel approach to soft robotic gripper design, as shown in Fig. 1, targeting at both aforementioned challenges, towards high-payload performance while preserving compliance, as well as sensory feedback, without requiring dedicated sensors. the main contributions are as follows:

- Proposed a novel POSA joint including multiple active actuators and a single passive actuator, with position and force proprioception. While generating higher grasping forces, proprioception could be achieved using the
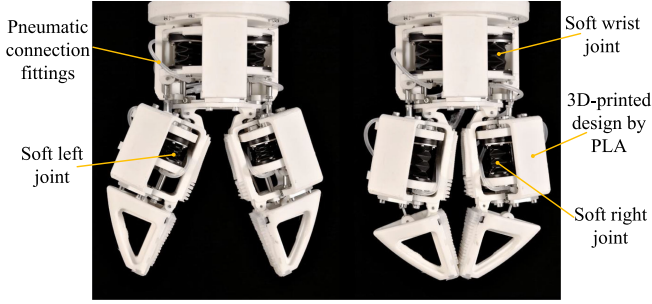
Fig. 1. The proposed high-payload proprioceptive hybrid robotic gripper driven by soft origamic actuators.
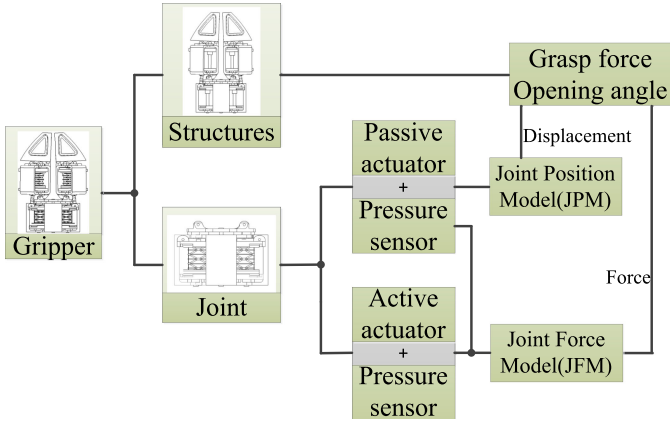

Fig. 2. The overall block diagram of our proposed method.

embedded cost-efficient air pressure sensors in the pneumatic control loop.

- Proposed a novel high-payload hybrid gripper based on the proposed joint, with two fingers and three degrees of freedom (DOF). Combing the compliance of soft robotic actuators and the high payload origamic structure, the gripper could work in two modes: *DELICATE MODE* and *POWER MODE*, with performances validated experimentally.
- Force and displacement proprioception based on the proposed model and embedded pressure sensors was enabled on the proposed gripper, and validated with experimental results on the proprioception-based position control of the hybrid gripper, as well as the recognition of objects with different sizes and weights.

II. SYSTEM OVERVIEW AND DESIGN APPROACH

A. Proprioception Principle and Overall Approach

The system overview of the high-payload hybrid gripper with position and force proprioception is shown in Fig. 2. The gripper consists of two main components: a soft-actuator joint and rigid supporting structures as motion constraints. Air pressure sensors are installed in the driving unit for sensing the movement and external stimulations.

TABLE I
GEOMETRY PARAMETERS OF THE ACTUATOR

H	The initial height	40.00mm
h	The initial height of one element	15.75mm
t	Thickness of the actuator	1.20mm
α_0	The initial dihedral angle of two trapezoid facets	90°
D	Diameter of circumcircle of cross section	40.00mm
a	Length of short parallel side of trapezoid	4.78mm
b	Length of long parallel side of trapezoid	32.72mm

A passive soft actuator was placed in each joint, for the measurement of inner-chamber air pressure during operations. Based on the Joint Position Model (JPM), deformation caused by external stimulation could be monitored by the changes of inner pressure. Forces exerted on the object of the gripper is generated from POSA joint. It includes both active and passive actuators, all of which are evenly installed in parallel between the two ends of POSA joint. The force comes from two parts for each actuator: pressure difference between inner actuator and atmosphere, and the self-deformation. The pressure in the active actuator is changed by the air pump, while the pressure in passive one is changed by the movement of POSA joint. All of them can be measured by the embedded air pressure sensors directly. Due to all actuators installed in parallel in the joint, they have the same axial deformation measured indirectly by the air pressure sensor installed in the passive actuator based on JPM. By combining pressure information of passive and active actuator, the force exerted on the object can be perceived based on the Joint Force Model (JFM). The pressure sensor alone could provide sufficient information for coding the movement and force detection of the gripper.

B. Actuator Design

An origamic actuator has been proposed, as shown in Fig. 3a, with one DOF linear translation along its axis [24], the principle geometry parameters are shown in Table I. The repetitive trapezoid facets leads to simple design of geometric parameters for customization and stable linear movement. Both the actuator body and the bottom cover are manufactured by molding of Polypropylene rubber. An air vent at the top of the actuator is designed to connect to pneumatic fittings.

An analytical model of the actuator is derived based on the geometric parameters, to capture the relations between the output force, inner pressure and axial displacement:

$$l = \sqrt{2}nh \sin\left(\frac{\alpha}{2}\right), \tag{1}$$

where l is the axial length of the actuator with H as the initial value before deformation. α is the dihedral angle of two trapezoid facets with α_0 as the initial value. n is the number of origami layer; and the rest of notations can be referred in Table I. The contraction ratio β can be derived:

$$\beta = \frac{H - l}{H} = 1 - \frac{\sqrt{2}nh \sin(\alpha/2)}{H}, \tag{2}$$

The output force is generated from two parts: (1) the self deformation of each actuator (2) the pressure difference between
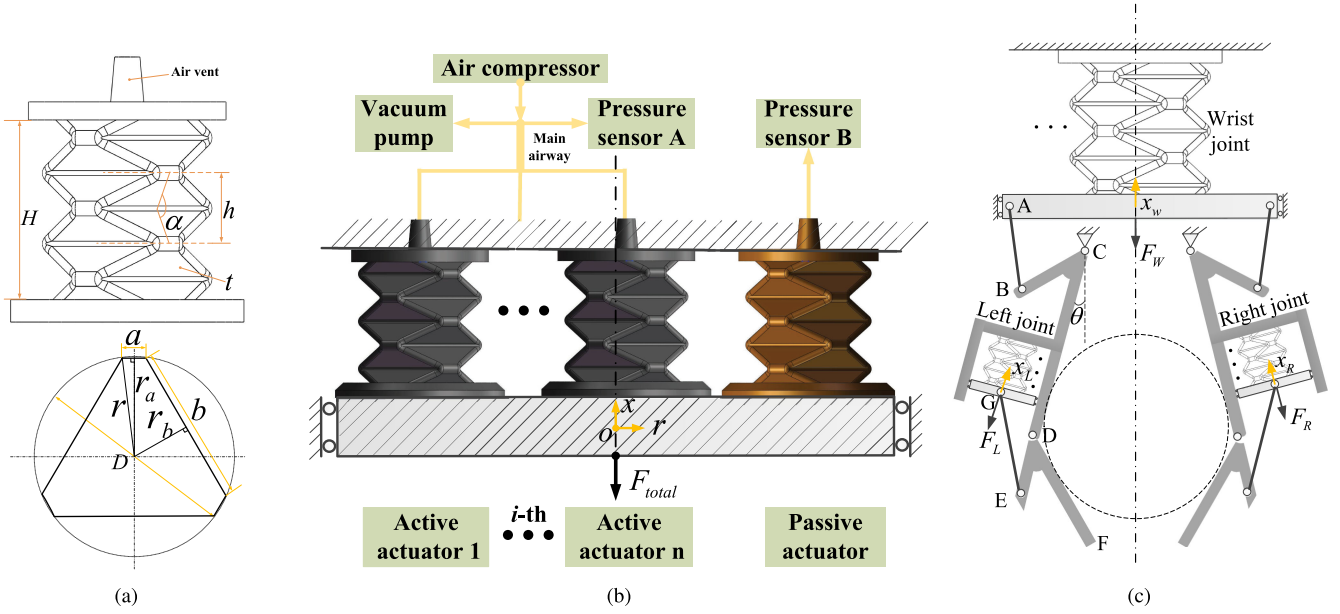
Fig. 3. (a) top: The proposed soft actuator and its geometry parameters; bottom: the cross section; (b) The scheme of proposed parallel actuator. The black and brown actuator are the active actuator and passive actuator respectively. Pressure sensor A is connected to the main airway and pressure sensor B is inserted into air vent of actuator directly. F_{total} is the output force; (c) The scheme of proposed soft robotic gripper.

the inner chamber and atmosphere.

$$F = F_d(\beta) + F_s(P_m), \tag{3}$$

where P_m is relative pressure in the inner chamber, $F_d(\beta)$ is a function of the contraction ratio and can be modeled experimentally, $F_s(P_m)$ is a function of P_m. It can be derived from $F_s = SP_m = \frac{\pi D_e^2}{4\epsilon}P_m$. S is the effective area of the actuator, D_e is the equivalent diameter approximated by $D_e = r_a + r_b$ and ϵ is obtained experimentally.

To improve force output, multiple soft actuators are placed in parallel, forming a POSA joint, as shown in Fig. 3b. Each joint comprises of N actuated (active) actuators and 1 passive actuator, with the passive actuator placed at the center surrounded by the N active ones. The pneumatic pressure sensor connected to the passive actuator measures pressure changes in the actuator chamber, and estimates the distance between the two joint planes based on equation (3), while the total force (JFM) could be derived as follows:

$$F_{total} = \sum_{i=1}^{n} F_i + F_p$$

$$F_i = \frac{\pi D_{ei}^2}{4\epsilon_i} P_{mi} + g_i(x)$$

$$F_p = \frac{\pi D_{ep}^2}{4\epsilon_p} P_{mp} + g_p(x), \tag{4}$$

where F_i and F_p are the output forces generated from each of the N active actuators and the 1 passive actuator, respectively. P_{mi} is inner relative pressure of the i-th active actuator, while P_{mp} is that of the passive actuator. The axial displacement is $x = H - l$. Specifically, $x = 0$ when the actuator is at the equilibrium position.

In this scenario, the air in the passive chamber is assumed ideal, therefore Boyle's law could be followed as:

$$P \propto \frac{1}{V}, \tag{5}$$

with the absolute pressure P exerted by a given mass of an ideal air inversely proportional to the volume V occupied within a closed system.

$$(P_0 + P_a) V_0 = (P_{mp} + P_a) V$$

$$V = \frac{\pi D_e^2}{4} (H - x), \tag{6}$$

where P_0 and V_0 are the initial relative pressure and the volume of the chamber, respectively. P_a is the atmospheric pressure. By combining the two equations in equation (6), the relation (JPM) between the axial displacement and the inner pressure can be derived:

$$\frac{P_0 + P_a}{(P_{mp} + P_a)\epsilon_{s1}} + \frac{x}{H\epsilon_{s2}} = 1, \tag{7}$$

where ϵ_{s1} and ϵ_{s2} are the scale factors introduced to correct the equation and can be calibrated experimentally.

C. Gripper Design

The proposed hybrid robotic gripper is presented in Fig. 3c. It consists of one wrist joint and two fingers. Each finger has two links, i.e. proximal link and distal link sequentially connected by two hinges to the wrist. The wrist joint drives two fingers simultaneously around corresponding fixed hinges (C for left finger) using two mirror-imaged offset slider-crank mechanisms. The distal link of each finger is actuated by the finger joint, respectively, around each distal joint using a smaller offset slider-crank mechanism. Here, offset slider-crank mechanisms
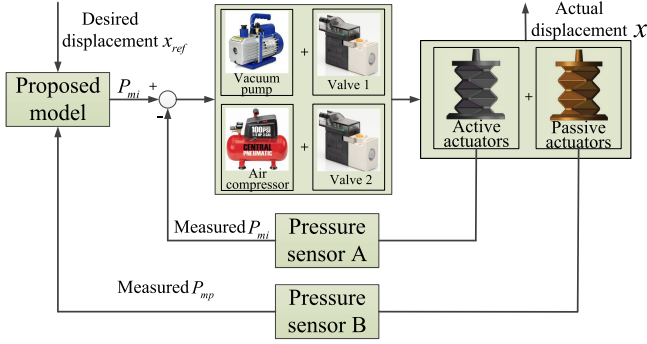
Fig. 4. The proposed displacement control scheme of the joint.

are used for the extended opening range of the fingers. Thus, the gripper has 3-DOFs driven by POSA pneumatic parallel origamic actuators along with auxiliary components and pneumatic ttings, dexterous enough to grasp objects with various shapes and sizes. The axial displacement x_W, x_L and x_R and the output force F_W, F_L and F_R of each joint can be measured by JFM to achieve force and displacement proprioception.

To be specific, the wrist joint can be driven along the axis by pressure, which is used to rotate the two fingers around the fixed hinge (hinge C). This arrangement increases the opening range of the gripper. When the two fingers touch the objects, the contacting points of the fingers stays at the position, the continuing inflation of actuator results in higher output force leading to tight grasps. The smaller finger actuator installed on the wrist joint makes the distal finger rotate around Distal joint D (left finger) to regulate the grasp displacement more precisely. Moreover, this two-finger design allows the gripper to conform to large convex-shape objects with stable contact. Furthermore, not only the output force but also the friction coefficient will be the crucial condition to lift the heavier objects. In consideration of this principle, to further improve the performance when picking up heavy objects, soft contact interface layer fabricated by silicone rubber are fixed on the finger bellies to increase friction. Besides, to deal with light small objects, which are relatively difficult to accomplish for conventional gripper, a triangular protrusion is designed at point F.

III. CONTROL AND ACTUATION

A. Control Strategy

Compliance is the most important characteristic which enables the robot to adapt to unstructured environment and interacting with uncertainty. In this work, a three-loop control approach was used for the proposed gripper: (1) outer loop: grasping force and opening angle control for the gripper; (2) middle-loop: the force and displacement control for each joint; (3) inner loop: pressure control for each active actuator, as shown Fig. 4. The control frequency for the overall control loop is 20 Hz. The middle loop obtains the desired displacement x_{ref}, from the opening angle of the fingers from the outer loop and the feedback from the pressure sensor in the passive actuator, providing pressures of the active actuators regulated by the inner loop.

B. Pressure Control

To drive the actuator to the desired position, the inner-loop pressure control as shown in Fig. 4, follows the dynamic pressure model derived in equation (5) and (6):

$$\dot{P} = -\frac{P}{V}\dot{V} + \frac{kRT}{V}\dot{m}$$

$$\dot{V} = -\frac{\pi D_e^2}{4}\dot{x}, \tag{8}$$

where k, T, $\dot{m}$ are the specific heat ratio (1.4 for ideal air), temperature and mass flow rate in the circuit, respectively. $\dot{m}$ relates to the valve orifice determined by the applied control signal u and the source pressure P_{pr} as follows.

$$\dot{m} = Q(P_{pr}, u), \tag{9}$$

Cost-effective solenoid valve are used to control the air flow. To match with the binary control actions, a deadzone-enhanced binary controller is utilized, eliminating oscillations caused by chattering as reported previously in [8].

C. Displacement Control

To reduce the control error of displacement and increase robustness, displacement of the passive actuator is utilized for control, as shown in Fig. 4, estimated by equation (7) from the air pressure sensor installed in the passive actuator. The initial pressure P_{mi0} can be given by:

$$P_{mi0} = w(x_{ref}), \tag{10}$$

where the function w can be learned from the experimental results. Through the measured displacement $x_{measured}$, the actual input pressure in the inner loop can be rearranged as:

$$P_{mi} = P_{mi0} + \gamma \Delta P_{mi}, \tag{11}$$

where γ is the regulatory factor. In our control strategy, the increment of P_{mi} for every time step can be given $\Delta P_{mi} = P_{mi0}\frac{x_{ref}-x}{x_{ref}}$. It will be positive when $x_{ref} - x > \xi$ (the threshold value given by specific task), or negative when $x_{ref} - x < -\xi$. When $|x_{ref} - x| < \xi$, the desired displacement is considered as achieved.

IV. EXPERIMENTS VALIDATION

A. Actuator and Joint Performances

To implement the proposed model in equations (4) and (7), stiffness of actuators, ϵ_{s1}, ϵ_{s2}, ϵ_i and ϵ_p were calibrated by experiments in Fig. 5a. Actuators can contract or elongate smoothly along the linear rails (HIWIN-MGN7H, 146.8 mm max.). They were driven by a step motor (6400 steps per revolutions), connecting the linear motion platform to the slider. The axial deformation of actuator could be monitored by a linear potentiometer (Miran 100 mm, 0.5 mm resolution) fixed on the slider as displacement sensor. Force sensor installed at the end of the slide measured the tensile and compressive force generated from the actuator. Supporting frames were 3D-printed by polylactic acid (PLA).
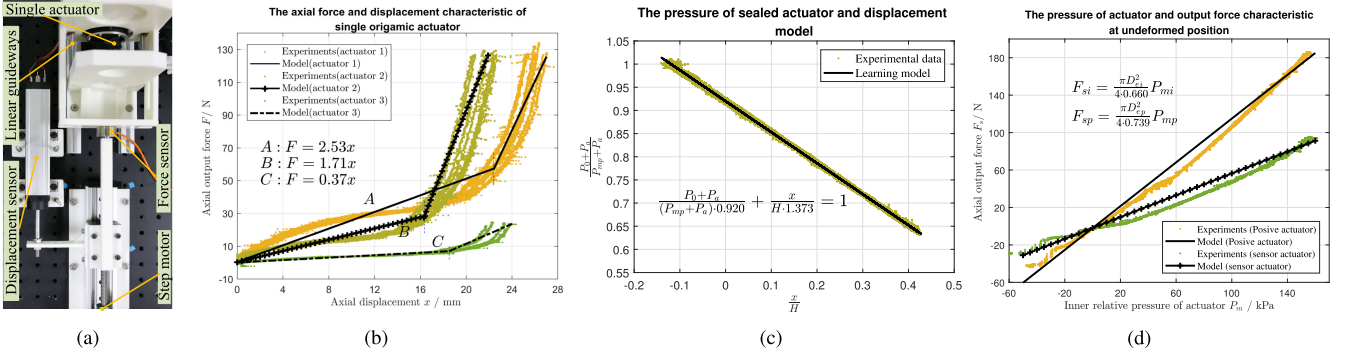
Fig. 5. (a) Experiment set up for single muscle. (b) Function g in equation (4) is modeled from the experimental data. Its gradient is the approximated stiffness coefficient of the single actuator. (c) The calibrated parameters ϵ_{s1}, ϵ_{s2} in equation (7) can be computed from the figure. (d) The parameter ϵ in $F_s(P_m)$ can be computed at undeformed position ($x = 0$ mm).
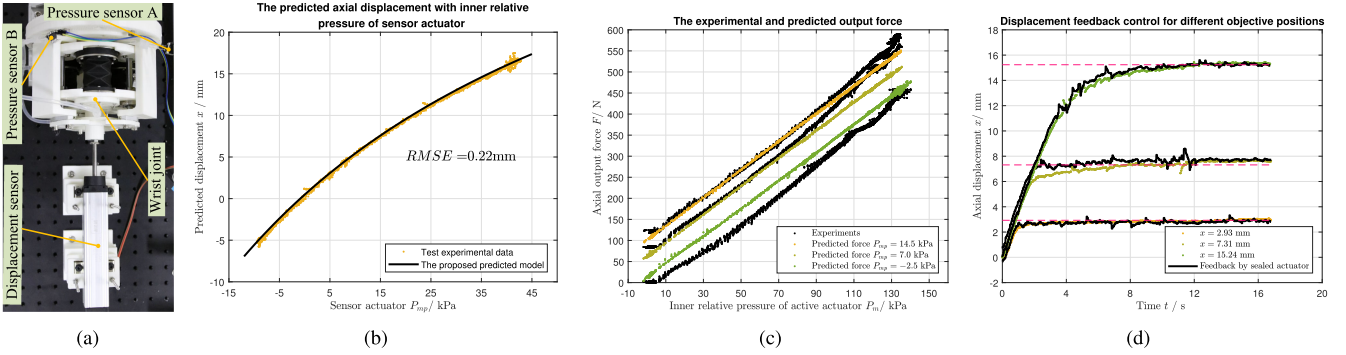

Fig. 6. (a) Experiment set up for joint. (b) The axial displacement predicted by our proposed model. (c) The axial predicted output force of joint at three different positions. (d) Displacement control for three different reference positions.

To select appropriate actuators, three single actuators based on Table I with slightly different parameters (actuator 1, 90 Shore A, $D = 40$ mm; actuator 2, 90 Shore A, $D = 20$ mm; actuator 3, 70 Shore A, $D = 20$ mm. Shore A: The measure of the hardness of rubber) were tested (Fig. 5b). Actuator 1 and Actuator 2 could generated the larger force compared to Actuator 3 within the same contraction. To improve the output force and enable the gripper more compact, Actuator 1 and Actuator 2 were selected as active actuator and sensory actuator, respectively. Relation between inner pressure of actuator and its axial displacement was experimented by connecting an air pressure sensor to the apparatus in Fig. 5a. From Fig. 5c, the non-dimensional inner pressure related linearly to non-dimensional axial displacement. Hence, the parameters $\epsilon_{s1} = 0.920$ and $\epsilon_{s2} = 1.373$ in equation (7) can be obtained. Moreover, by changing pressure of the actuator using a vacuum pump or air compressor with solenoid pneumatic valve (working pressure range: 0–7 bar) at the equilibrium position, relation between active inner pressure and the output force could be derived (Fig. 5d). The calibrated parameters for the active and passive actuators were obtained, $\epsilon_i = 0.66$, $\epsilon_p = 0.739$. From equation (4) and (7), the total force $F_{total}(P_m, P_{mp})$ and displacement x could be obtained.

The evaluated experiments to validate the accuracy of the proposed model was set up in Fig. 6a. This joint was a POSA joint

with three active actuators monitored by pressure sensor A (SS-CDANN060PAAA5, 413 kPa, Digi-Key) and one sensory actuator measured by pressure sensor B (SSCDANN030PAAA5, 206 kPa, Digi-Key). They were powered by 3.3 V DC. Bellow of the joint was connected to a force sensor or a displacement sensor as a reference to validate our predicted outputs. The performance of our proposed model was presented in Fig. 6b and Fig. 6c. RMSE of the predicted displacement equaled 0.22 mm. The average of predicted displacement error was 0.2%. The axial output force F_{total} of the single joint reached 564.5 N at $P_m = 130$ kPa. The force prediction error averaged 5.6%.

Since the characterization of the three joints of the gripper were very similar, the only test on the three reference positions for the wrist joint was listed here as shown in Fig. 6d. The joint was able to follow the reference signal with the convergence time of 1 s, 4 s,12 s for the three position 2.93 mm, 7.31 mm, 15.24 mm respectively. Its position error could reach as low as 3.21%.

B. Gripper Performance Validation

The fabricated gripper was shown in Fig. 7a. Its key geometry parameters were presented in Table III. The main structural components were 3D-printed by PLA. The gripper contains
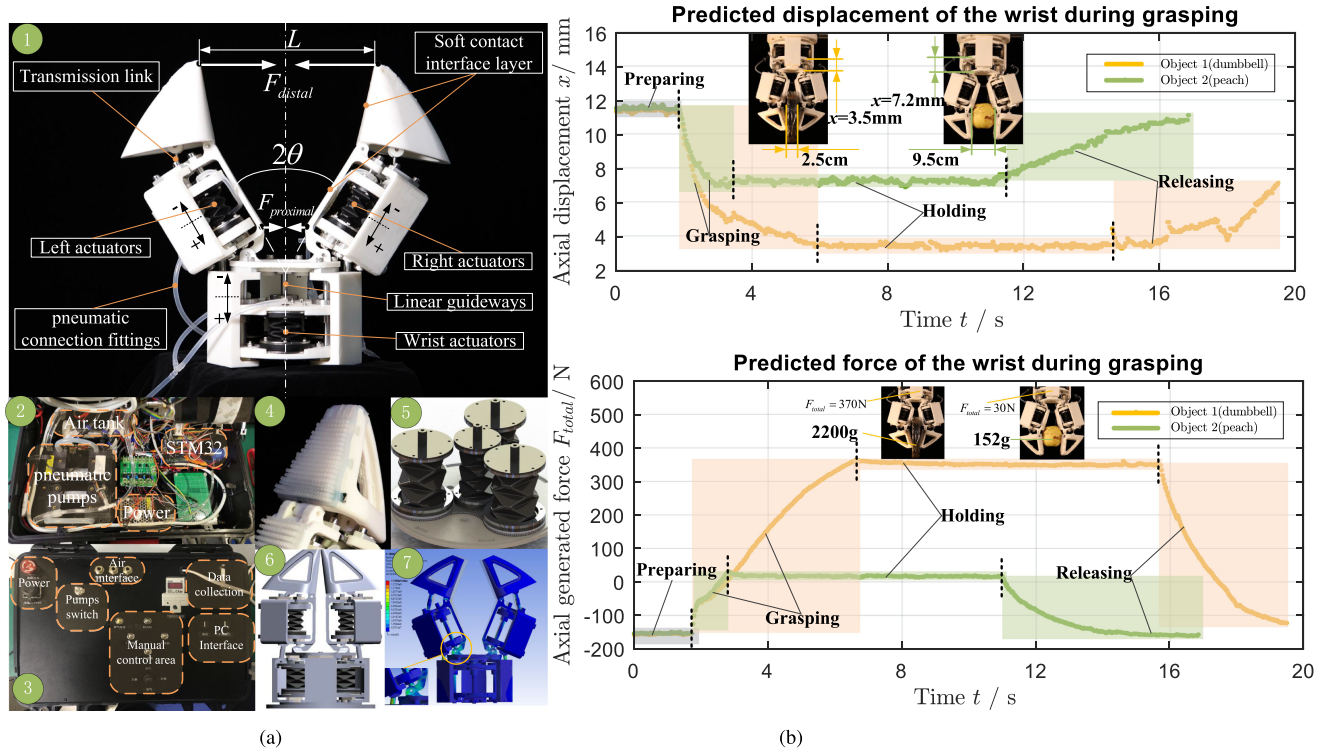
Fig. 7.   (a.1) The proposed fabricated robotic gripper. (a.2 and a.3) The dedicated control box and control penal. (a.4) Finger covered with contact interface layer. (a.5) The actuators distribution for joint wrist. (a.6) 3D model. (a.7) Static characteristics by FEM. (b) Proprioception for dumbbell and peach.

three joints, including a three-active one-passive POSA wrist joint and two-active one-passive POSA finger joints. The active actuators of the wrist were Actuator 1 in Fig. 5b, while the two active actuators of each finger were Actuator 2. Actuator 2 were also used as the sensory actuators for all joints measured by air pressure sensors. The linear guideways installed in each joints ensure the actuators output only linear translation. When pressure in the active actuator equaled atmospheric pressure, the actuators stayed at the equilibrium position, corresponding to the closed position of two fingers.

The control system for the gripper was designed, as shown in Fig. 7a.2 and Fig. 7a.3. It contained pneumatic pumps, control unit STM32, power source, air tank, the valve unit, and other support sections, all of which were integrated into the $400 \times 300 \times 180$ millimeter box weighing 4.4 kg. To improve the efficiency and safety of the gripper, two air tanks and related feedback controls were considered. In this way, the air pressure source with a specified value can be set in advance. It also had two different control interfaces: manual control by control buttons and PC control by the PC interface.

To adapt to various surface types of the object and increase reliability of grasping, a soft contact layer was fixed on the finger surfaces, as shown in Fig. 7a.4. The layer was filled with small cylindrical lattices distributed evenly to prevent the lateral slip of the objects. Protruding structures were placed along the edge are used to connect to the gripper. It was cast by 20 Shore A silicone rubber. The edge was cast with 5 Shore A silicone rubber, which can adapt to the shape of the object in case of the lateral slip.

The distal effective displacement of L for two fingers could reach up to 305 mm when the opening angle stretches the maximum $2\theta = 84°$. The large grasping range provided feasibility of grasping objects with a variety of size. To test the grasping force, the force sensor (measuring range:0-1000 N) was mounted between the two fingers at the distal and proximal position. The maximum proximal grasping force $F_{proximal}$ equaled 302.4 N with pressure of the wrist joint at $P_m = 135$ kPa, while maximum distal force F_{distal} equaled 52.1 N with the joint and finger pressure at $P_m = 135$ kPa and $P_m = 90$ kPa respectively.

Two representative objects (dumbbell, peach) with different sizes and weights were tested on the dedicated experimental platform to validate the function of this proposed robotic gripper. In the tests, pressure sensors were the only measurements to monitor the inner chamber pressures of the actuators. Each grasping trial included four stages: *preparing,grasping, holding,* and *releasing*. Based on the proposed model in equation (4) and (7), the measured pressure of grasping objects were employed to obtain position and force proprioceptive estimations, as shown in Fig. 7, where the four grasping stages were marked by different translucent rectangular frames. At the holding stage, for the larger size peach, the gripper required a wider displacement as $x = 7.2 \pm 0.3$ mm from the wrist joint, while the smaller dumbbell required $x = 2.5 \pm 0.3$ mm, as shown in Fig. 7 top. Regarding grasping force, to grasp the heavier object dumbbell required at least $F_{total} = 370$ N at the wrist, compared to $F_{total} = 30$ N for the lighter peach, as shown in 7 bottom. It was worth noting that the gripper could differentiate the smaller

TABLE II
COMPARISON OF THE PROPOSED GRIPPER DESIGN AND PREVIOUS WORKS

	BCL-4 [25]	BCL-6 [10]	BCL-13 [15]	Bellows hybrid gripper [26]	Our proposed gripper
Fingers	2	3	4	2	2
DOFs	4	6	13	1	3
Self-weight	0.2kg	0.4kg	1.27kg	-	3.2kg
Actuators	Bellows actuator	Ellipse-shaped bending actuator	3-DOF soft pneumatic actuator	Bellows actuator	Origamic actuator
Grasping force	Joint: 50N, Distal: 12N	40N	9.6N	6N	Joint: 564.5N, Proximal: 302.4N, Distal: 52.1N
Proprioception	No	No	No	By air pressure senor based on antagonistic actuator	By air pressure senor based on the POSA joint

TABLE III
KEY GEOMETRY PARAMETERS OF THE GRIPPER

AB	BC	CD	DE	EG	DF	$2\theta_{max}$
50mm	25mm	119mm	51mm	40mm	92mm	84°

but heavier object from the larger but lighter object effectively with the proposed force and position proprioception approach.

The comparisons between the proposed gripper and previous works was shown in Table II. Combining soft actuator compliance, high force capability, and position/force proprioception, the proposed hybrid robotic gripper was capable of gasping heavy payload while attaining the desirable compliant characteristics of soft robotic grippers. In particular, two grasping modes were demonstrated for the gripper: a *DELICATE MODE* where it could hold fragile or small objects without causing damage; and a *POWER MODE* where it could apply strong forces sufficient to hold heavy objects or crush eggs and walnuts, otherwise highly challenging for soft grippers. In addition, the gripper could switch flexibly between the two modes by simultaneously tracking the position and force signals enabled by the proposed proprioception approach, thus adapting to a wide range of grasping tasks, as demonstrated in the supplementary video.

V. CONCLUSION AND FUTURE WORK

In this letter, a high-payload two-finger hybrid robotic gripper with position and force proprioception was proposed, driven by the novel POSA joint with parallel origamic soft actuators and reinforced by 3D-printed rigid frames. A soft contact interface layer molded by silicone rubber on the fingertip was also introduced to improve contact stability. The two main objectives of this proposed design: strength and proprioception, were both effectively achieved: when fully pressurized, the proposed hybrid gripper could generate substantially larger forces than conventional soft robotic grippers, with the maximum $F_{proximal} = 302.4$ N and $F_{distal} = 52.1$ N; on proprioception, the minimum perceivable displacement and force errors could reach 0.2% and 5.6%, respectively; the maximum displacement control error could reach 3.21%; and it could perceive different size and weight of objects like dumbbell and peach. The desirable feature of passive compliance was preserved, despite the substantially increased strength, as demonstrated through grasping a range of delicate objects.

Future directions include: design optimization to further reduce the size and weight; control algorithm iteration to improve dynamic performance; and further development of the proprioception algorithm to enrich the feature set as well as improving functionality. This work demonstrated the feasibility of using embedded sensors on soft pneumatic robots to enable proprioception, leading to a new approach in developing simple, effective, and lost-cost soft and hybrid robots with advanced object handling capabilities. This will pave the way to a much wider aspect of robotic application in object handling tasks.

REFERENCES

[1] G. J. Monkman, S. Hesse, R. Steinmann, and H. Schunk, *Robot Grippers*. Hoboken, NJ, USA: Wiley, 2007.

[2] L. Chin, M. C. Yuen, J. Lipton, L. H. Trueba, R. Kramer-Bottiglio, and D. Rus, "A simple electric soft robotic gripper with high-deformation haptic feedback," in *Proc. Int. Conf. Robot. Autom.*, 2019, pp. 2765–2771.

[3] J. Hughes, U. Culha, F. Giardina, F. Guenther, A. Rosendo, and F. Iida, "Soft manipulators and grippers: A review," *Frontiers Robot. AI*, vol. 3, 2016, Art. no. 69.

[4] S. Kim, C. Laschi, and B. Trimmer, "Soft robotics: A bioinspired evolution in robotics," *Trends Biotechnol.*, vol. 31, no. 5, pp. 287–294, 2013.

[5] P. Polygerinos, Z. Wang, K. C. Galloway, R. J. Wood, and C. J. Walsh, "Soft robotic glove for combined assistance and at-home rehabilitation," *Robot. Auton. Syst.*, vol. 73, pp. 135–143, 2015.

[6] Y. Su, Y. Wang, and A. Kheddar, "Sample-efficient learning of soft task priorities through bayesian optimization," in *Proc. IEEE-RAS 18th Int. Conf. Humanoid Robots*, 2018, pp. 1–6.

[7] S. Li *et al.*, "A vacuum-driven origami magic-ball soft gripper," in *Proc. IEEE Int. Conf. Robot. Autom.*, 2019, pp. 7401–7408.

[8] P. Polygerinos *et al.*, "Modeling of soft fiber-reinforced bending actuators," *IEEE Trans. Robot.*, vol. 31, no. 3, pp. 778–789, Jun. 2015.

[9] D. Rus and M. T. Tolley, "Design, fabrication and control of soft robots," *Nature*, vol. 521, no. 7553, pp. 467–475, 2015.

[10] J. Zhou, S. Chen, and Z. Wang, "A soft-robotic gripper with enhanced object adaptation and grasping reliability," *IEEE Robot. Autom. Lett.*, vol. 2, no. 4, pp. 2287–2293, Oct. 2017.

[11] J. Yi *et al.*, "Customizable three-dimensional-printed origami soft robotic joint with effective behavior shaping for safe interactions," *IEEE Trans. Robot.*, vol. 35, no. 1, pp. 114–123, Feb. 2018.

[12] T. Park and Y. Cha, "Soft gripper actuated by electro-hydraulic force," in *Proc. SPIE, Electroact. Polym. Actuat. Devices (EAPAD) XXI*, International Society for Optics and Photonics, 2019, pp. 236–241.

[13] T. Park, K. Kim, S.-R. Oh, and Y. Cha, "Electrohydraulic actuator for a soft gripper," *Soft Robot.*, vol. 7, no. 1, pp. 68–75, 2020.

[14] P. Nakkarat and S. Kuntanapreeda, "Observer-based backstepping force control of an electrohydraulic actuator," *Control Eng. Pract.*, vol. 17, no. 8, pp. 895–902, 2009.

[15] J. Zhou, J. Yi, X. Chen, Z. Liu, and Z. Wang, "BCLl-13: A 13-DOF soft robotic hand for dexterous grasping and in-hand manipulation," *IEEE Robot. Autom. Lett.*, vol. 3, no. 4, pp. 3379–3386, Oct. 2018.

[16] X. Chen, J. Peng, J. Zhou, Y. Chen, M. Y. Wang, and Z. Wang, "A robotic manipulator design with novel soft actuators," in *Proc. IEEE Int. Conf. Robot. Autom.*, 2017, pp. 1878–1884.

[17] E. A. Peraza-Hernandez, D. J. Hartl, R. J. Malak Jr, and D. C. Lagoudas, "Origami-inspired active structures: A synthesis and review," *Smart Mater. Struct.*, vol. 23, no. 9, 2014, Art. no. 094001.

[18] J. Yi, X. Chen, C. Song, and Z. Wang, "Fiber-reinforced origamic robotic actuator," *Soft Robot.*, vol. 5, no. 1, pp. 81–92, 2018.

[19] J. Shintake, V. Cacucciolo, D. Floreano, and H. Shea, "Soft robotic grippers," *Adv. Mater.*, vol. 30, no. 29, 2018, Art. no. 1707035.

[20] P. Glick, S. A. Suresh, D. Ruffatto, M. Cutkosky, M. T. Tolley, and A. Parness, "A soft robotic gripper with gecko-inspired adhesive," *IEEE Robot. Autom. Lett.*, vol. 3, no. 2, pp. 903–910, Apr. 2018.

[21] W. Wang and S.-H. Ahn, "Shape memory alloy-based soft gripper with variable stiffness for compliant and effective grasping," *Soft Robot.*, vol. 4, no. 4, pp. 379–389, 2017.

[22] M. Luo *et al.*, "Toward modular soft robotics: Proprioceptive curvature sensing and sliding-mode control of soft bidirectional bending modules," *Soft Robot.*, vol. 4, no. 2, pp. 117–125, 2017.

[23] T. Helps and J. Rossiter, "Proprioceptive flexible fluidic actuators using conductive working fluids," *Soft Robot.*, vol. 5, no. 2, pp. 175–189, 2018.

[24] Y. Guo, X. Chen, and Z. Wang, "Environmental insulation of 3d printable origamic soft actuators," in *Proc. 9th IEEE Int. Conf. CYBER Technol. Autom., Control, Intell. Syst.*, 2019, pp. 1–6.

[25] J. Zhou, X. Chen, J. Li, Y. Tian, and Z. Wang, "A soft robotic approach to robust and dexterous grasping," in *Proc. IEEE Int. Conf. Soft Robot.*, 2018, pp. 412–417.

[26] L. Wang and Z. Wang, "Mechanoreception for soft robots via intuitive body cues," *Soft Robot.*, to be published, doi: 10.1089/soro.2018.0135.